Exploitation of Triangular Lattice Arrays for Improved Spectral Efficiency in Massive MIMO 5G Systems

Francesco Alessio Dicandia, Member, IEEE, Simone Genovesi, Senior Member, IEEE
Dipartimento di Ingegneria dell'Informazione, University of Pisa, Pisa, 56122, Italy
Corresponding author: Simone Genovesi (e-mail: simone.genovesi@unipi.it).

ABSTRACT A thorough analysis of the performance of planar arrays with a regular periodic lattice is carried out and applied to massive multiple-input-multiple-output (MIMO) systems operating within 5G NR n257 and n258 frequency band. It is shown that, among different arrangements with uniform spacing, a triangular lattice guarantees the reduction of the Average Side Lobe Level (ASLL), a better angular scan resolution of the main beam within a predefined angular sector and a lower mutual coupling level among elements. Moreover, single beam and multibeam application scenarios are considered for the performance comparison and both cases assess the remarkable features offered by a triangular arrangement. Particular attention is paid to illustrate, for different propagation channel scenarios, the effects of the array lattice on overall system performance including average gain as well as Signal-to-Interference plus Noise Ratio (SINR) and Sum Spectral Efficiency (SSE). The obtained results prove that a regular and periodic triangular lattice is appealing for arrays to be adopted in massive MIMO 5G systems.

INDEX TERMS Antenna array, 5G, massive MIMO, multibeam antenna, broadband array.

I. INTRODUCTION

Massive multiple-input-multiple-output (MIMO) can offer a significant boost to the throughput of 5G wireless communication systems [1]–[4]. In general, there are three main factors that affect the throughput of the network: bandwidth, cell size and Spectral Efficiency (SE) [3]. In the past, different approaches have been adopted to cope with the ever increasing data traffic, such as recurring to larger bandwidths or deploying more base stations to reduce the cell area [5]. In contrast, in the upcoming 5G generation, the improvement of the data throughput is guaranteed primarily by the massive MIMO technology able to increase the SE by serving multiple users simultaneously in the same time-frequency resource through Spatial Multiplexing (SM) [6]. The implementation relies on a base station array with a massive number of antennas that use concurrently multibeam to send to separate users the different streams of data allocated on the same time-frequency resource [7]. Among the frequency bands that will be dedicated to 5G communications, the mm-wave spectrum has recently attracted a large interest because of the limited available spectrum below 6 GHz [8]–[10]. In fact, the large spectrum available at mm-wave can support wide bandwidth signals

and hence high data throughput in 5G communication systems [11]. However, despite the advantage of a large spectrum, mm-wave signals experience some impairments with respect to those below 6 GHz [12], such as more severe propagation loss, rapid channel fluctuation with a reduction of the coherence time, significant power consumption in the analog-to-digital (A/D) conversion as well as a low power amplifier efficiency. On the other hand, a small wavelength allows compact antenna arrays with a large number of elements thus ensuring a high antenna directivity useful to balance the higher path loss as well as to support multiple users [10]. Different antennas array for mm-wave have been proposed [13] to exploit these features. For example, phased arrays working at 28 GHz with 32 and 64 elements have been proposed in [14], [15] respectively. Both solutions are based on 2×2 transmit/receive (TRX) beamformer chips that allow attaining a single beam steering with a maximum scan angle of 50° in azimuth and 25° in elevation. In [16] a massive MIMO system, composed by 64 elements with a fully digital beamforming for 5G mm-wave communication operating at 28 GHz, has been realized and tested. To double the channel capacity, dual polarized phased array transceivers have been also designed [17], [18] to provide

two concurrent independent beams.

A challenging task for large phased array at mm-wave is represented by the cooling system for dissipating heat [19], [20]. Passive cooling systems are preferred to active ones from industry since they do not need electricity. From the antenna array perspective, the simplest way to help the cooling system to dissipate the heat is to increase the distance among antenna elements [20]. However, increasing too much the inter-element spacing could lead to grating lobes or high lateral lobes inside the visible region. This effect is very harmful in terms of Signal-to-Interference Ratio (SIR) in case of multi-user communication at the same time-frequency resource. Most of the designed array solutions for massive MIMO rely on square or rectangular array architectures with a uniform lattice. However, in [21] it was showed that a potential increase in the channel capacity can be obtained by exploiting an irregular antenna array layout. Planar array topologies based on irregular layouts have been designed by using convex optimization technique with the aim of decreasing the Peak-Side-Lobe-Level (PSLL) [22]–[25]. It has to be observed that the reduction of the PSLL by aperiodic arrangements is obtained by spreading the energy in a larger solid angle, thus raising the Average Side Lobe Level (ASLL) [26] with a consequent maximum array gain reduction. Moreover, these irregular array solutions based on an extensive optimization procedure present some challenges in terms of practical design increasing considerably the complexity of the feeding network [27], [28].

Among the mm-wave frequency bands that will be committed to 5G wireless communications, the most promising are the 5G New Radio (NR) n258 band (24.24 GHz – 27.5 GHz) and the 5G NR n257 band (26.5 – 29.5 GHz). Few antenna array solutions are able to cover both these frequency bands such as the wideband dual-polarized solution exploiting a tightly-coupled dipole array [29], [30]. However, as mentioned before, having elements too close each other can drastically worse the thermal aspect and hence complicate the cooling system of the transceiver, in addition to having lower angular resolution to resolve the users [3] and high antenna elements mutual coupling (MC) able to drastically undermine the massive MIMO performance [31], [32].

It is also interesting to notice that massive MIMO antenna array are mostly implemented by using square or rectangular arrangements among the elements [14], [15], [17], [18], [33] although the triangular lattice may exhibit several advantages. In fact, it not only allows using fewer antenna elements than the same array with a square lattice [34], but it enables to avoid the premature appearance of grating lobes as well as a larger distance among array antenna elements [35]. In [36] a 8×8 phased array with the radiating elements placed in a equilateral triangular lattice has been presented. This array operates in the 5G NR n257 band and it can steer the beam up to 60° off broadside. However, a comprehensive

analysis addressing the overall performance, including massive MIMO metrics, for an array with triangular lattice has not yet been addressed.

The purpose of this paper is to assess the benefit of adopting a triangular lattice in order to improve massive MIMO 5G performance in terms of average gain, minimum distance among elements (d_{min}), ASLL and SE within both the 5G NR n257 and n258 band. The obtained results prove that a triangular arrangement of the array elements provide significant advantages with respect to other regular lattices. Moreover, the triangular lattice exhibits a higher degree of versatility in serving users distributed in differently shaped sector cells. It worthwhile to note that, although the analysis has been focused within both 5G NR n257 and n258 band, it is possible to infer that the performance enhancement offered by triangular lattice planar arrays could be also exploited in other frequency bands as well as applications where the massive MIMO technology is employed.

The comparison between an equilateral triangular lattice and a square one is presented in Section II by analysing a planar array of 8×8 elements and considering the gain and PSLL as a function of the angular beam steering. The following Section III is devoted to find the most suitable triangular lattice in terms of array gain and minimum antenna element spacing and to comparing the results with respect to a rectangular lattice planar array. Multibeam antennas serving users in a predefined angular sector through independent directive beams are addressed in the Section IV. Massive MIMO system metrics, such as SINR and SE, are evaluated in Section V for planar arrays comprising 64 elements (8×8) and compared in case of equilateral and isosceles triangular lattice as well as square and rectangular ones. Conclusions are summarized in Section VI.

II. EQUILATERAL TRIANGULAR VS SQUARE LATTICE PLANAR ARRAY

Let us consider a planar array composed by $N \times M$ elements. The array radiation pattern (RP) is given by [37]:

$$RP(\theta,\phi) = \sum_{n=0}^{N-1} \sum_{m=0}^{M-1} I_{nm} e^{j\varphi_{nm}} E_{nm}(\theta,\phi) e^{j\beta F} \quad (1)$$

$$F = x_{nm} \sin(\theta)\cos(\phi) + y_{nm} \sin(\theta)\sin(\phi)$$

where $\beta = 2\pi/\lambda_0$ is the phase constant, $E_{nm}(\theta,\phi)$ represents the element radiation pattern, I_{nm} is the excitation amplitude and φ_{nm} the phase associated to the (n,m)-th element whose position (x_{nm}, y_{nm}) depends on the employed lattice. In case of triangular lattice (Fig. 1), the radiation pattern (RP_{tri}) can be seen as a superposition of the fields generated by two displaced rectangular lattices, RP_r and RP_g [38].

In particular, by considering an isotropic element factor (i. e. $E_{nm}(\theta,\phi) = 1$) the RP_{tri} is given by:

$$RP_{tri}(\theta,\phi) = RP_r(\theta,\phi) + RP_g(\theta,\phi)$$

$$RP_r(\theta,\phi) = \sum_n \sum_m e^{j\varphi_{nm}} e^{j\beta A}$$

$$A = 2n\Delta X \sin(\theta)\cos(\phi) + m\Delta Y \sin(\theta)\sin(\phi)$$

$$\begin{cases} n = 0,1,2,\cdots, N/2-1 \to N = even \\ n = 0,1,2,\cdots, (N-1)/2 \to N = odd \end{cases} ; \quad m = 0,1,2\cdots, M-1$$

$$RP_g(\theta,\phi) = \sum_n \sum_m e^{j\varphi_{nm}} e^{j\beta B}$$

$$B = \left[2n\Delta X + \Delta X\right]\sin(\theta)\cos(\phi) + \left[m\Delta Y + \Delta Y/2\right]\sin(\theta)\sin(\phi)$$

$$\begin{cases} n = 0,1,2,\cdots, N/2-1 \to N = even \\ n = 0,1,2,\cdots, (N-1)/2-1 \to N = odd \end{cases} ; \quad m = 0,1,2\cdots, M-1$$

$$(2)$$

where $RP_r(\theta,\phi)$ and $RP_g(\theta,\phi)$ represents the *RP* of the red and the green planar array, respectively.
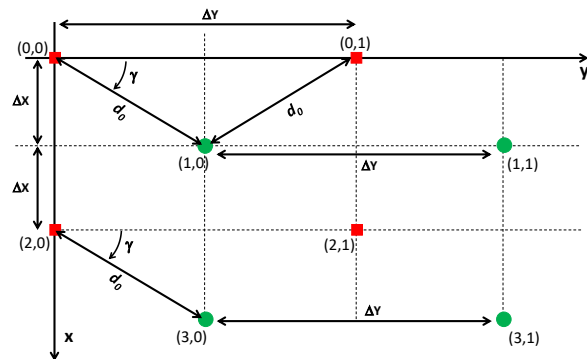

FIGURE 1. Planar array with triangular lattice. The two rectangular lattices are highlighted by the red and green dots and generate the far field *RP_r* and *RP_g*, respectively.

The spacing (*ΔX*, *ΔY*) represents the height and the base of the triangle and are related to the angle γ by the following equations:

$$\begin{cases} \Delta X = d_0 \sin(\gamma) \\ \Delta Y = 2d_0 \cos(\gamma) \end{cases} \quad (3)$$

where d_0 is the hypotenuse of the right-angled triangle, namely the distance between the (*n,m*)-*th* element and the (*n+1,m*)-*th* element (Fig. 1). The phase (φ_{nm}) associated to the (*n,m*)-*th* element necessary to steer the beam toward the desired direction (u_0,v_0) is equal to:

$$\begin{aligned} \varphi_{nm} &= \beta\left(x_{nm}u_0 + y_{nm}v_0\right) \\ u_0 &= \sin(\theta_0)\cos(\phi_0) \\ v_0 &= \sin(\theta_0)\sin(\phi_0) \end{aligned} \quad . \quad (4)$$

Although the equilateral triangle lattice (γ = 60°) is the most common adopted arrangement, isosceles triangular lattices (γ≠60°) can be considered for improving the array overall performance. In view of exploring different element dispositions, the array gain and the PSLL of the equilateral triangular case (γ = 60°) have been evaluated within the visible region as a function of the beam steering inside a defined angular sector. Regarding the sector where the main

beam is steered to serve the users, it is assumed to span 30° in elevation and 120° in azimuth as shown in Fig. 2, which is currently considered for typical 5G sector scenario [25], [39]. Once selected the array lattice, the distance between elements is a crucial parameter since it affects the appearance of grating lobes inside the visible region during the beam steering and hence the array gain, ASLL and PSLL.

To avoid the appearance of grating lobes inside the visible region, the minimum distance among elements (d_{min}) in the case of a square lattice has to satisfy the following condition:

$$d_{\min} \leq \frac{\lambda_{HF}}{1 + \sin(\theta_{0,\max})} \quad (5)$$

where λ_{HF} represents the wavelength in free space at the highest frequency (29.5 GHz) and $\theta_{0,max}$ the maximum steering angle of the array between the elevation and azimuth plane, which is 60° for the sector shown in Fig. 2. Conversely, in the case of an equilateral triangular (γ = 60°) arrangement, the minimum distance d_{min} turns out to be $2/\sqrt{3}$ times wider than the square lattice [35]. Therefore, the minimum element distance goes from 0.53 λ_{HF} in the case of square lattice to 0.618 λ_{HF} for the equilateral triangular one.
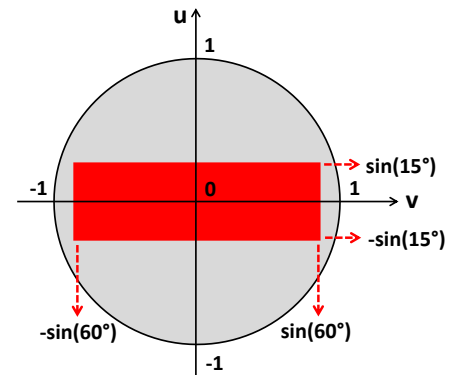

FIGURE 2. Rectangular sector within which the main beam of the planar array is steered.

A triangular lattice therefore guarantees a larger minimum distance (d_{min}) between elements and thus a lower level of Mutual Coupling (MC). This can contribute to improve the stability of the antenna element input impedance during the beam steering, to better exploit the linear regime of the employed Power Amplifiers (PAs) and, more in general, a lower degradation of the massive MIMO performance [31], [32].

An 8×8 array is shown in Fig. 3 for both equilateral triangular (γ = 60°) and square lattice. The triangular lattice occupies a greater area than square one due to a larger minimum spacing d_{min}. This causes a better angular resolution and, in a multiusers scenario, a reduced angular interval within which users cannot be spatially resolved [3]. The larger element distance of the triangular lattice can be also considered in favor of a better heat dissipation that is critical in large mm-wave phased array [20] .
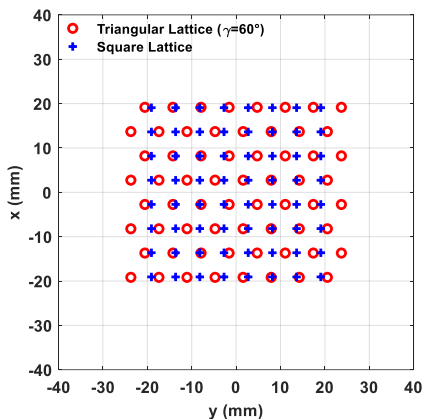
IEEE *Access*
Multidisciplinary : Rapid Review : Open Access Journal

FIGURE 3. Array comprising 64 elements: red dots refer to equilateral triangular layout (γ = 60°) whereas blue crosses to a square lattice.

The array gain in dBi and PSLL in dB as a function of the main beam direction (u_0, v_0) inside the rectangular sector are illustrated in Fig. 4 for both the triangular lattice and the square one for an isotropic element factor (*i.e.* $E_{nm}(\theta,\phi) = 1$). By comparing the results reported on the color maps, it can

be noticed that both the employed array lattices exhibit similar trend during the beam steering within the investigated bandwidth even though the triangular lattice (γ = 60°) allows obtaining higher gain values than square one. The array gain presents higher values along broadside direction and decreases during the main beam steering due to the beam widening as well as to the approaching of the grating lobes inside the visible region [37]. Moreover, the PSLL maps confirm that the selected antenna elements distance avoids the appearance of grating lobes during the beam scan and they approach the visible region ($\theta = 90°$) only at the highest frequency (Fig. 4 c,f). In fact, at 24.25 GHz and 26.875 GHz (Fig. 4a,d and d,e) a PSLL of around −13 dB is guaranteed for whole the investigated sector for both the employed lattices. On the contrary, at the highest frequency (Fig. 4 c,f) in case of deep main beam steering angles the grating lobes beam starts to move into the visible region with a consequent reduction of the PSLL.

For a more comprehensive analysis, the impact of the employed lattice on array gain has been also evaluated from a statistical point of view.
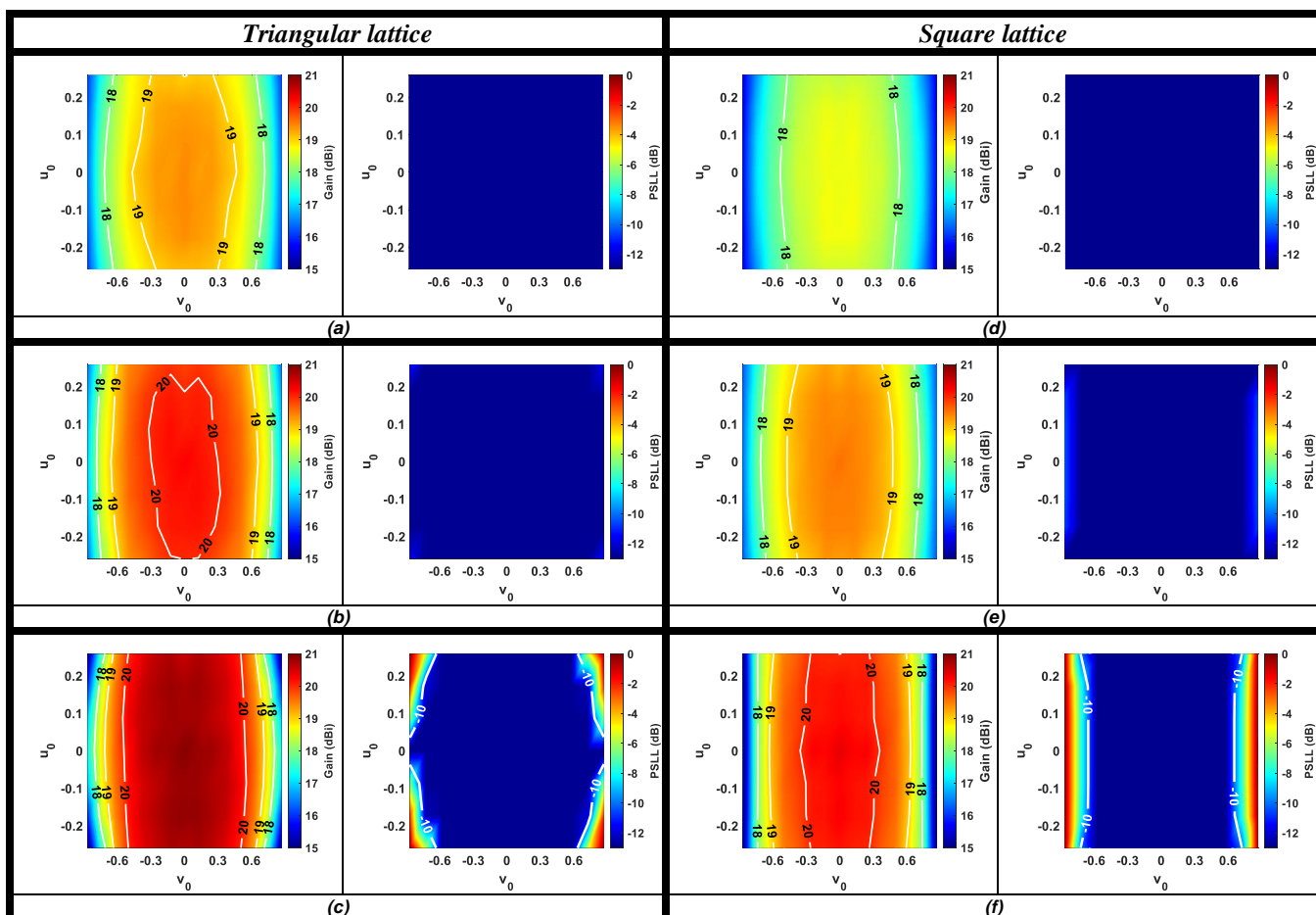

FIGURE 4. Color maps reporting the array gain in dBi and the PSLL in dB scale as a function of the main beam direction (u_0, v_0) inside the defined sector in case of a planar array with 8×8 elements. Gain (left) and PSLL (right) in case of triangular lattice (γ = 60°) at *(a)* 24.25 GHz, *(b)* 26.875 GHz and *(c)* 29.5 GHz; gain (left) and PSLL (right) in case of square lattice at *(d)* 24.25 GHz, *(e)* 26.875 GHz and *(f)* 29.5 GHz.

More in detail, the mean value (η_{Gain}), the minimum value (min_{Gain}) and maximum value (max_{Gain}) of the gain as a function of the frequency are calculated and reported in Fig. 5. It is apparent that the equilateral triangular lattice outperforms the square one. In fact, the equilateral triangular grid allows a percentage improvement of the mean gain (η_{Gain}) in dBi between $3.28 - 3.75$ % with respect to the square one within the whole n257 and n258 frequency band ($24.25 - 29.5$ GHz). Moreover, it can be drawn that the triangular lattice ($\gamma = 60°$) provides higher maximum value (max_{Gain}) and minimum value (min_{Gain}) of the gain than square one.

The array gain values ensured by triangular lattice enable to obtain higher Signal-to-Noise Ratio (SNR) for each user served inside the sector as well as a lower ASLL by exploiting a better focus of the main beam. These factors lead to a significant improvement of the Signal-to-Noise plus Interference Ratio (SINR) with a consequent enhancement of the wireless communication performance as will be addressed in the following.
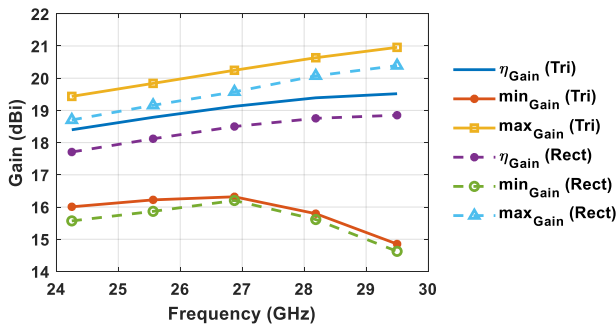

FIGURE 5. Array gain statistical comparison between triangular ($\gamma = 60°$) and square lattice planar array of an array of 8x8 elements as a function of the frequency.

III. ISOSCELES TRIANGULAR VS RECTANGULAR LATTICE PLANAR ARRAY

So far, only equilateral triangular arrangement ($\gamma = 60°$) and square one have been considered and compared. However, it is possible to select different values of γ and search for better array configurations. In general, for a triangular lattice, the grating lobe absence conditions are given by:

$$\left(\frac{\lambda}{2\Delta X} - u_{0,max}\right)^2 + \left(\frac{\lambda}{\Delta Y} - v_{0,max}\right)^2 \geq 1 \quad (6)$$

$$\frac{2\lambda}{\Delta Y} - v_{0,max} \geq 1 \quad (7)$$

$$\frac{\lambda}{\Delta X} - u_{0,max} \geq 1 \quad (8)$$

where ΔX and ΔY represents the height and the base of the triangle shown in Fig. 1 whereas $u_{0,max}$ and $v_{0,max}$ are the maximum steering angles where the main beam is steered to serve the users along elevation and azimuth plane respectively, namely $u_{0,max} = \sin(15°)$ and $v_{0,max} = \sin(60°)$ according to the sector shown in Fig. 2. Therefore, by

considering (6)-(8), the spacings ΔX and ΔY such that during the beam steering inside the rectangular sector do not cause grating lobes, are equal to:

$$\frac{\lambda}{\left(\sqrt{\alpha^*} + v_{0,max}\right)} \leq \Delta Y \leq \frac{2\lambda}{\left(1 + v_{0,max}\right)} = \Delta Y_{max} \quad (9)$$

$$\Delta X \leq \frac{\lambda}{2\left(u_{0,max} + \sqrt{1+\alpha}\right)} \quad (10)$$

where

$$\alpha = \left(\lambda_{HF}/\Delta Y - v_{0,max}\right)^2 \quad (11)$$

$$\alpha^* = \left[\lambda_{HF}/\left(2\Delta X_{max}\right) - u_{0,max}\right]^2 \quad (12)$$

$$\Delta X_{max} = \lambda_{HF}/\left(1 + u_{0,max}\right) \quad (13)$$

By considering the previous ΔY spacing range (9) along with the maximum ΔX spacing (10), the γ value regarding the triangular lattice turns out to be $36.6° \leq \gamma \leq 70.7°$. For the other γ values for triangular lattice, the array elements spacing (ΔX, ΔY) that do not provide grating lobes inside the visible region are given by:

$$if \ \gamma < 36.6° \begin{cases} \Delta X = \dfrac{\Delta Y \tan(\gamma)}{2} \\ \Delta Y = \Delta Y_{max} \end{cases} \quad (14)$$

$$if \ \gamma > 70.7° \begin{cases} \Delta X = \Delta X_{max} \\ \Delta Y = \dfrac{2\Delta X}{\tan(\gamma)} \end{cases} \quad (15)$$

It is worthwhile to notice that only isosceles triangle lattices with different γ values are considered since the scalene one has a lower minimum distance (d_{min}) between elements. To understand the effect of γ on the triangular lattice of the considered 8×8 planar array, the average gain (η_{Gain}) in dBi has been evaluated by considering the rectangular sector (Fig. 2) for a γ value included from $20°$ to $80°$. As the color map of Fig. 6 emphasizes, the γ value has a significant effect on the average gain.

More in detail, lower frequencies turn out to be more sensitive to γ value by showing an average gain variation up to 17 % whereas, with the increasing of the frequency, the average gain is more stable. Moreover, γ values greater than $70°$ and lower than $30°$ provide a steep reduction of the gain at all the frequencies. In order to identify an optimal γ value a frequency average of the η_{Gain} has been calculated within the addressed bandwidth ($24.25 - 29.5$ GHz) and it is reported in Fig. 7.
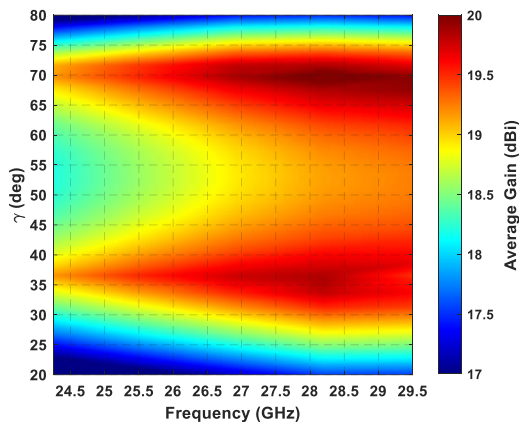
FIGURE 6. Average gain (η_{Gain}) in dBi as a function of the frequency by considering different values of γ in case of triangular lattice planar array of 8x8 elements.
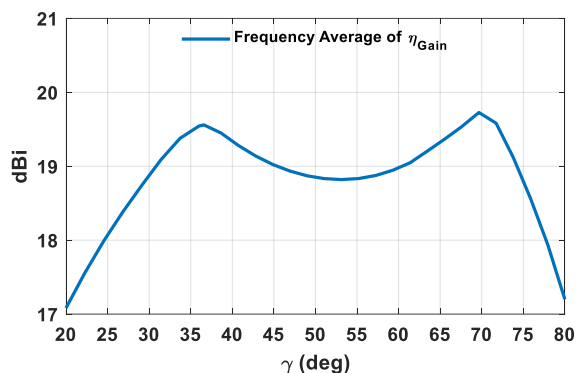

FIGURE 7. Frequency average of the η_{Gain} as a function of the γ value of the triangular lattice in case of a planar array of 8x8 elements.

From Fig. 7 it can be drawn that at the beginning the frequency average of the η_{Gain} increases almost linearly up to γ = 36.6° then it gently decreases with the increasing of the γ value up to around γ = 55° where an exchange of the trend occurs. Afterwards, the frequency average of the η_{Gain} reaches the maximum value around γ = 70° after which it quickly decreases. However, since the minimum distance among elements (d_{min}) is of paramount importance for the performance, it is reported in Fig. 8 as a function of the γ value.
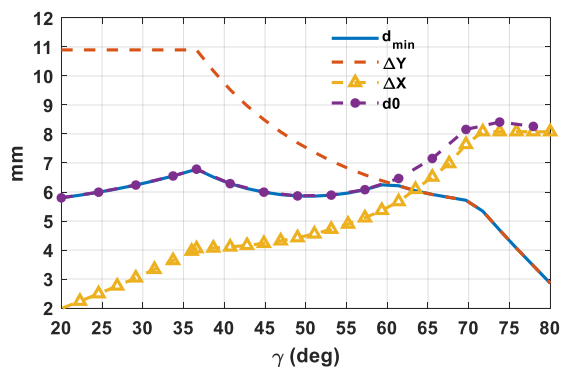

FIGURE 8. Minimum elements distance (d_{min}), elements spacing (ΔX,ΔY) and d_0 as a function of the γ value for the triangular lattice.

As it is apparent, although γ = 70° allows to reach the highest frequency average of η_{Gain} (Fig. 7) it does not guarantee the largest minimum value of d_{min}. In fact, this is achieved at the first peak of the frequency average of the η_{Gain}, namely γ = 36.6° (d_{min} = 6.788 mm). Furthermore, γ = 36.6° ensures also the largest ΔY spacing providing the highest spatial resolution along v plane, namely the azimuth plane where the greater angular coverage of 120° occurs. Therefore, it is reasonable to infer that, γ = 36.6° represents the best choice regarding the isosceles triangular lattice by considering the rectangular sector shown in Fig. 2 since it is able to provide the largest minimum elements spacing, the highest azimuth resolution as well as the greatest average gain among all γ values where ΔY > ΔX. Therefore, the gain reported in Fig. 6 and Fig. 7 as well as the antenna elements spacing of Fig. 8 emphasize that isosceles triangular lattice (γ≠60°) outperforms the equilateral triangular one (γ = 60°) in case of a rectangular sector.

Under the assumption of a rectangular sector with a coverage of 30° in elevation and 120° in azimuth (Fig. 2) it seems fair to compare the performance of the optimal isosceles triangular lattice (γ = 36.6°) with a rectangular lattice instead of a square one and with the same number of antenna elements (M = 64) arranged in the same form factor (8×8). In case of the rectangular lattice, the absence of grating lobes inside the visible region is ensured if the elements spacing along x and y axis satisfy the following equations:

$$d_x \leq \frac{\lambda_{HF}}{1+u_{0,\max}} \tag{16}$$

$$d_y \leq \frac{\lambda_{HF}}{1+v_{0,\max}} \tag{17}$$

where d_x and d_y represents the element spacing along x and y axis, respectively. Therefore, the rectangular lattice is obtained from the square one but increasing the elements distance along the x axis (d_x) namely the plane where occurs the lower angular coverage. The overlapped array geometry by using the isosceles triangular lattice (γ = 36.6°) with the spacing (ΔX, ΔY) shown in Fig. 8 and the largest rectangular grid according to (16)-(17) is illustrated in Fig. 9.

From Fig. 9 it can be seen that the isosceles triangular lattice provides higher spatial resolution along azimuth plane (y axis) than rectangular one. Therefore, the transformation from square to rectangular lattice provides a larger area and hence superior gain value, but the same resolution along azimuth plane (y axis) due to (17). On the contrary, the isosceles triangular lattice with γ < 60° allows improving spatial resolution along azimuth plane as previously shown in Fig. 8. Moreover, the minimum distance among elements in case of rectangular lattice remains exactly the same of the square one, namely d_{min} = 0.53 λ_{HF} = 5.44 mm because of (17) whereas the isosceles triangular arrangement of the elements allows to widen the elements spacing. In fact, the

minimum elements distance among elements goes from $d_{min} = 0.618 \, \lambda_{HF}$ for the equilateral triangular ($\gamma = 60°$) to $d_{min} = 0.667 \, \lambda_{HF} = 6.788$ mm for the isosceles ($\gamma = 36.6°$) one, by providing around 20 % wider minimum element spacing than rectangular or square lattice. A statistical gain comparison between the isosceles triangular ($\gamma = 36.6°$) and rectangular array lattice is shown in Fig. 10.
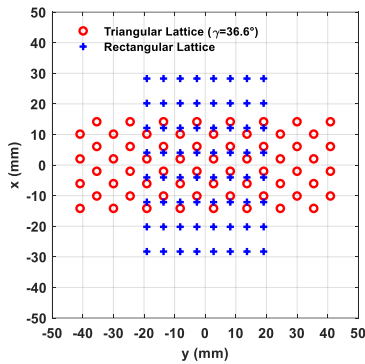

FIGURE 9. Array geometry composed by *M* = 64 elements (8×8) in case of isosceles triangular (γ = 36.6°) and rectangular lattice.

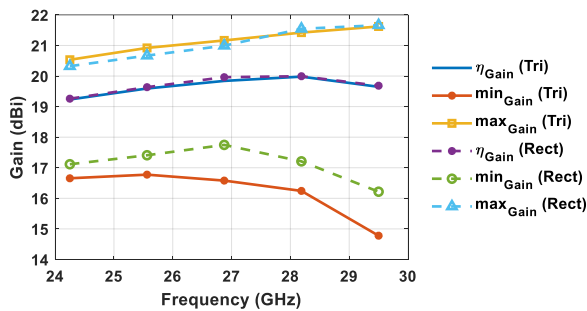**FIGURE 10.** Array gain statistical comparison between isosceles triangular (γ = 36.6°) and rectangular lattice planar array of 8×8 elements as a function of the frequency.

Unlike the comparison between equilateral triangular and the square lattice gain (Fig. 5), isosceles triangular and rectangular lattice exhibits similar performance. In fact, the optimal isosceles triangular lattice ($\gamma = 36.6°$) guarantees a slightly higher maximum gain value at the lower frequencies but in general it is characterized by an average gain value inside the rectangular sector comparable to the rectangular lattice. Moreover, the rectangular lattice outperforms the isosceles triangular one in terms of minimum gain value inside the rectangular sector.

Since in massive MIMO systems the user's interference plays a key role and represents the performance bottleneck, it is worth making a performance comparison by considering the ASLL inside the sector. From Fig. 11 can be drawn that isosceles triangular lattice enables decreasing the mean value of the ASLL (η_{ASLL}) for all the frequencies inside the sector with respect to rectangular lattice although the two lattices provide similar average gain (Fig. 10). This feature is attractive in massive MIMO 5G systems since it allows reducing both the intra-cell interference as well as the inter-

cell interference. In fact, the side lobes related to the main beam pointing at one user causes interference towards all other users in the same time-frequency resource.
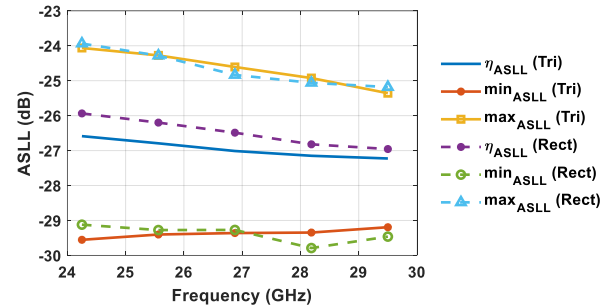

FIGURE 11. ASLL statistical comparison between isosceles triangular (γ = 36.6°) and rectangular lattice planar array of 8x8 elements as a function of the frequency.

IV. MULTIBEAM ANTENNA

So far, the comparison among triangular, square and rectangular lattice has been carried out in terms of gain and ASLL within a defined sector. However, in the upcoming 5G wireless technology, the improvement of the data throughput will be provided by multibeam antenna [40] which can create several concurrent and independent directive beams. Various beamforming methods are available to achieve multibeam [7], [10], [16], [41], [42]. Among all, the fully-digital beamforming solution represents the best performance although requiring a different radio frequency chain for each antenna element [43].

The normalized multibeam radiation patterns of the isosceles triangular lattice ($\gamma = 36.6°$) and the rectangular one are illustrated in Fig. 12 for two configurations of five users located inside the highlighted sector evaluated at the lowest operation frequency (24.25 GHz) since it provides the largest angular interval within which users may be spatially not resolved in case of multi user's scenario. In the former configuration (*conf#1*) the users are located at: [$u_1 = 0°, v_1 = -\sin(55°)$], [$u_2 = 0°, v_2 = -\sin(40°)$], [$u_3 = 0°, v_3 = 0°$], [$u_4 = 0°, v_4 = \sin(30°)$], [$u_5 = 0°, v_5 = \sin(60°)$] whereas in the latter (*conf#2*) the users are situated at: [$u_1 = \sin(15°), v_1 = -\sin(60°)$], [$u_2 = -\sin(5°)°, v_2 = -\sin(40°)$], [$u_3 = 0°, v_3 = -\sin(10°)$], [$u_4 = \sin(15°), v_4 = \sin(35°)$], and [$u_5 = \sin(10°), v_5 = \sin(55°)$]. Moreover, the multibeam radiation pattern was achieved through the Maximum Ratio (MR) linear precoding and combining algorithm being the most powerful and computationally efficient beamforming method [5], [25]. It is worth noting that the phase difference among the array antenna elements retrieved through the MR algorithm necessary to create the concurrent beams can be implemented with all the beamforming methods (analog, digital or hybrid) with the respective performance limits.

As it is evident from the color maps of Fig. 12, isosceles triangular lattice (Fig. 12*a,c*) makes the antenna beams more focused towards the users than rectangular one (Fig. 12*b,d*) by exploiting the improved angular resolution. In fact, in

case of rectangular lattice, all the five users are not always served by a well-defined independent beam thus producing a degradation of the SIR and hence of the overall wireless 5G performance.
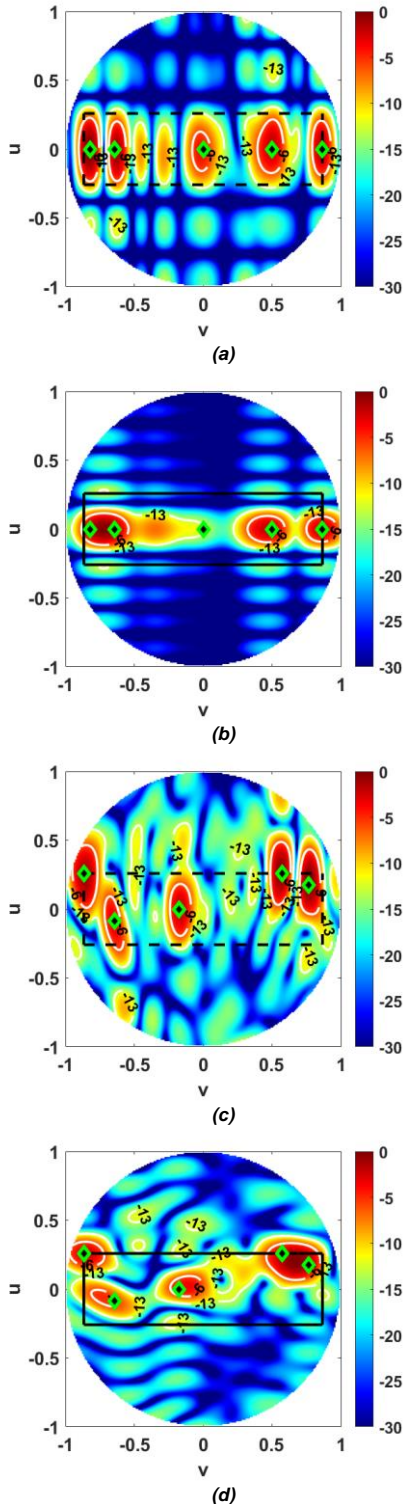

FIGURE 12. Normalized multibeam radiation pattern in dB at 24.25 GHz of a planar array with 8x8 elements in case of five users; *(a)* triangular lattice (γ = 36.6°) and *(b)* rectangular lattice in case of *conf#1* of the users; *(c)* triangular lattice (γ = 36.6°) and *(d)* rectangular lattice in case of *conf#2* of the users. Green/black diamond marker represents users' locations.

The improved performance of the optimal isosceles triangular lattice has been further confirmed by the SIR reported in Table I for both the user's configurations (*conf#1* and *conf#2*). By looking at the data of Table I, it is evident the better robustness to interference guaranteed by employing the triangular lattice array layout with respect to the rectangular one in case of MR beamforming algorithm.

Specifically, an improvement of the average SIR (η_{SIR}) of 5.44 dB for *conf#1* and 3.33 dB for *conf#2* with respect to rectangular lattice is obtained in case of five simultaneous users inside the defined sector and an isosceles triangular grid (γ = 36.6°) of the array antenna element. The η_{SIR} difference between triangular layout and rectangular one appears to be more evident in case of closer users, such as *conf#1*, and gradually decrease as the user's distance increase.

By considering the η_{SIR} of Table I and in case of interference-limited condition, namely at high SNR condition, the average SE for each user in case of isosceles triangular lattice is 5.19 b/s/Hz and 6.21 b/Hz/s for *conf#1* and *conf#2* situation respectively. On the contrary, by employing a rectangular lattice the average SE for each user is 3.47 b/s/Hz and 5.13 b/s/Hz [3].

TABLE I
SIR COMPARISON IN dB AT 24.25 GHz BETWEEN ISOSCELES TRIANGULAR LATTICE (γ = 36.6°) AND RECTANGULAR ONE

User	Conf#1			Conf#2		
	Tri	Rect	Diff	Tri	Rect	Diff
#1	14.23	6.07	8.16	22.1	20.29	1.81
#2	13.68	5.86	7.83	21.75	17.65	4.1
#3	17.34	14.59	2.75	22.32	17.36	4.96
#4	15.54	11.39	4.15	13.72	10.8	2.92
#5	16.7	12.39	4.31	13.43	10.56	2.78
η_{SIR}	**15.5**	**10.06**	**5.44**	**18.66**	**15.33**	**3.33**

V. SPECTRAL EFFICIENCY (SE)

Let us consider an isolated sector with a base station (BS) comprising $M_{bs} = 64$ (8×8) antenna elements that is serving K concurrent users equipped with a single isotropic antenna and. The received Signal-to-Interference-plus-Noise Ratio (SINR) for the nth user (ρ_n) can be written as [25], [44], [45]:

$$\rho_n = \frac{P_n |h_n \cdot w_n|^2}{\sum_{j=1, j \neq n}^{K} P_j |h_j \cdot w_n|^2 + \sigma_0} =$$

$$= \frac{\Gamma_n |h_n \cdot w_n|^2}{\sum_{j=1, j \neq n}^{K} \Gamma_j |h_j \cdot w_n|^2 + 1} \qquad (18)$$

where the numerator is the collected power by the nth user, the denominator corresponds to the received interference plus noise power (σ_0). P_n represents the transmitted power allocated for the nth user whereas Γ_n is defined as the ratio

between the transmitted power and the noise power ($\Gamma_n = P_n/\sigma_0$). More in detail, $h_n \epsilon\ 1 \times M_{bs}$ ($n = 1,2,..,K$) is a complex vector that corresponds to channel vector between the nth user and each antenna element of the BS whereas $w_n \epsilon\ M_{bs} \times 1$ consists of the precoding vector that depends on the selected beamforming method. Under the hypothesis of uniform transmitted power for each user ($\Gamma_n = \Gamma_0$, $n = 1,2,\ldots,K$) the received SINR for the nth user (ρ_n) can be written as:

$$\rho_n = \frac{\Gamma_0 G_n(\theta_n, \phi_n)}{\Gamma_0 \displaystyle\sum_{j=1,\, j \neq n}^{K} G_j(\theta_n, \phi_n) |h_j \cdot w_n|^2 + 1} \qquad (19)$$

where $G_n(\theta_n,\phi_n)$ represents the BS array gain toward the nth user located at (θ_n,ϕ_n). Once the SINR is known, the maximum achievable bit rate over 1 Hz of bandwidth for the nth user, namely the SE per user, is:

$$SE_n = \log_2\left(1 + \rho_n\right). \qquad (20)$$

To take into account the mutual coupling among array elements that undermines the MIMO performance [46], the massive MIMO channel matrix H is modeled as [47]:

$$H = G\left(I_{M_{bs} \times M_{bs}} - SS^H\right)^{1/2} \qquad (21)$$

where $G \epsilon\ K \times M_{bs}$ represents the complex channel gain among the users and the BS antenna elements in absence of antenna MC, $I_{Mbs \times Mbs}$ is a $M_{bs} \times M_{bs}$ identity matrix and $S \epsilon\ M_{bs} \times M_{bs}$ correspond to the S-parameters matrix of the BS array. So far, isotropic element factor was considered for selecting the most suitable planar array lattice, therefore a perfect input matching ($S_{ii} = 0$, $i = 1,2,\ldots,M_{bs}$) has been considered for S matrix. However, different array lattices provide dissimilar antenna elements spacing. Therefore the MC level between two elements as a function of the distance has been considered for the SE evaluation (Fig. 13) as illustrated in [48] to include this effect in the following analysis.
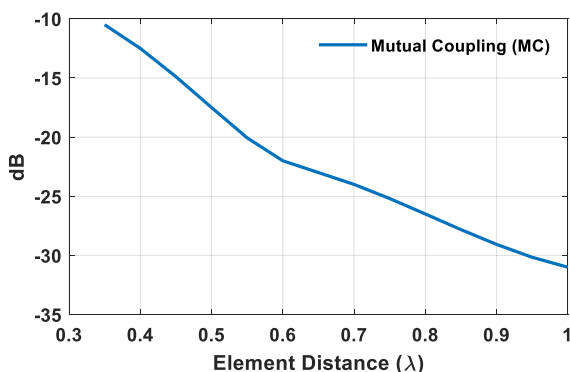

FIGURE 13. MC model in dB as a function of the elements spacing exploited for the calculation of the channel matrix H.

It is worth noting that, in general, the MC level depends also on the antenna elements typology employed to build the array. Therefore, the employed MC level (Fig. 13) was used just to extrapolate a general overview of the MC level independently from the kind of the antenna element.

By comparing the MC model of Fig. 13 and the above mentioned minimum distances among elements, it can be seen that the maximum MC level in case of square or rectangular lattice at the lowest frequency, namely 24.25 GHz, it turns out to be around −14.5 dB whereas the triangular arrangement of the antenna elements allow obtaining a maximum MC level of around −17.5 dB for the equilateral triangular lattice ($\gamma = 60°$) and −20 dB for the most suitable isosceles triangular one ($\gamma = 36.6°$).

A. LINE OF SIGHT (LOS)

Due to the severe path loss of the mm-wave channel communication as well as the employed highly directive antenna array beams, the line of sight (LOS) path represents the predominant mode of propagation between BS and users inside the sector with, in some cases, few non LOS (NLOS) multipath rays characterized by weaker channel gain [49]. This condition turns out to be further emphasized if users are equipped by multiple antenna elements.

To evaluate the performance of a massive MIMO systems, the sum rate SE (SSE) by serving K user simultaneously within the sector in LOS conduction has been calculated. More in detail, the MR beamforming technique and perfect CSI has been exploited for the SE evaluation. The SSE is calculated by using the following equation:

$$SSE = \sum_{k=1}^{K} E\left(\log_2\left(1 + \rho_k\right)\right) \qquad (22)$$

where $E(\cdot)$ represents the average operator. For the SSE assessment 10000 sets of K concurrent users uniformly distributed inside the rectangular sector were considered.

The SSE comparison in case of a $\Gamma_0 = 20$ dB is plotted in Fig. 14 as a function of the number of users (K) within the addressed frequency band. Specifically, Fig. 14a shows the comparison between equilateral triangular and square lattice whereas the SSE comparison in case of isosceles triangular grid and rectangular one is shown in Fig. 14b.

In general, by increasing the number of concurrent users, or equivalently the number of independent data streams, the SSE first increases rapidly, then tends to reach a maximum value. The first part, where the SSE growth is almost linear, is called *multiplexing regime* since the multiplexing gain outweighs the interference. Then, the SSE improvement slows down up to reaches the maximum in the *saturation regime*. Subsequently, for every additional user, the SSE tends to decrease.
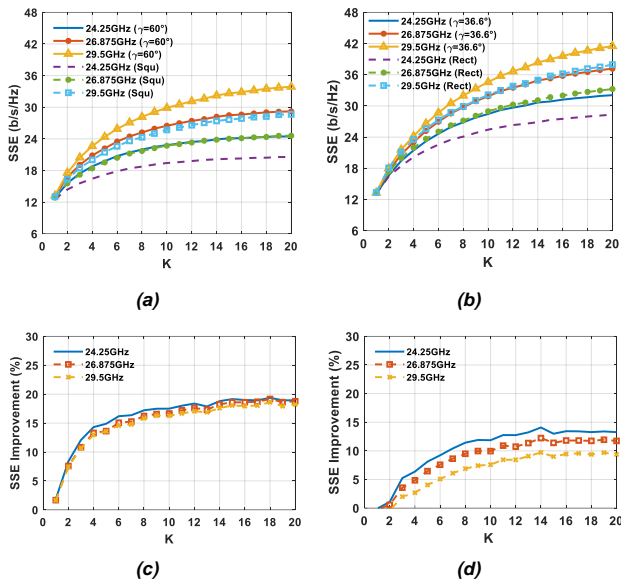
FIGURE 14. SSE comparison in case of a planar array composed by 8×8 elements and $\Gamma_0 = 20$ dB between *(a)* equilateral triangular ($\gamma = 60°$) and square lattice and *(b)* isosceles triangular ($\gamma = 36.6°$) and rectangular lattice. Percentage SSE improvement comparison between *(c)* equilateral triangular ($\gamma = 60°$) and square lattice and *(d)* isosceles triangular ($\gamma = 36.6°$) and rectangular lattice.

As it can be inferred from Fig. 14, for few users, namely at the beginning of the *multiplexing regime*, all the lattices provide similar SSE. However, with the increasing of the users, the SSE of triangular lattice outperforms the others. To better emphasize the SSE comparison, the percentage SSE improvement is calculated and reported in Fig. 14c,d where it is well visible the superior performance of the triangular lattice planar array within the addressed frequency band with respect to square or rectangular grids. More in detail, equilateral triangular lattice enables to achieve up to around 20 % more of the SSE than square lattice whereas, the isosceles triangular one guarantees up to a percentage improvement around 10 %– 14 % than rectangular grid in case of twenty users. Fig. 14c underlines higher SSE improvement than Fig. 14d since, unlike isosceles triangular lattice and rectangular one that are characterized by similar gain values inside the rectangular sector (Fig. 10), equilateral triangular lattice provides also a superior gain values with respect to square layout (Fig. 5) in addition to the better interference robustness guaranteed by the superior spatial resolution.

It is noteworthy to observe that the best SSE improvement occurs at the lowest frequency, namely where there is the highest antenna elements mutual coupling. This happens because the larger minimum distance among elements provided by the triangular lattice allows to undergo a lower SINR degradation due to the presence of the MC and hence it gives a considerable contribution to the SSE improvement. However, with the increasing of the frequency the MC tends to decrease, and therefore the greater distance guaranteed by triangular grid provides a lower improvement in percentage

than at the lowest frequency. This trend is confirmed through Fig. 15 where both the SSE and the percentage SSE improvement between the triangular lattice planar array ($\gamma = 36.6°$) and the rectangular one in case of MC and without MC (w/o MC) among array antenna elements has been shown. More in detail, from Fig. 15a,b it is well visible that the MC undermines the performance since it reduces the SSE with respect to ideal case without MC for both the investigated planar array lattices. The percentage SSE improvement in Fig. 15c highlights as the MC contributes to a further increase of the percentage SSE improvement of triangular lattice ($\gamma = 36.6°$) especially at the lowest frequency (24.25 GHz) where the array antenna elements are characterized by the highest MC level due to the shortest elements distance with respect to the wavelength. However, with the frequency increase the MC level fades little by little to become almost irrelevant at the highest investigated frequency (29.5 GHz) and therefore the percentage SSE improvement with and without MC tends to resemble more and more.
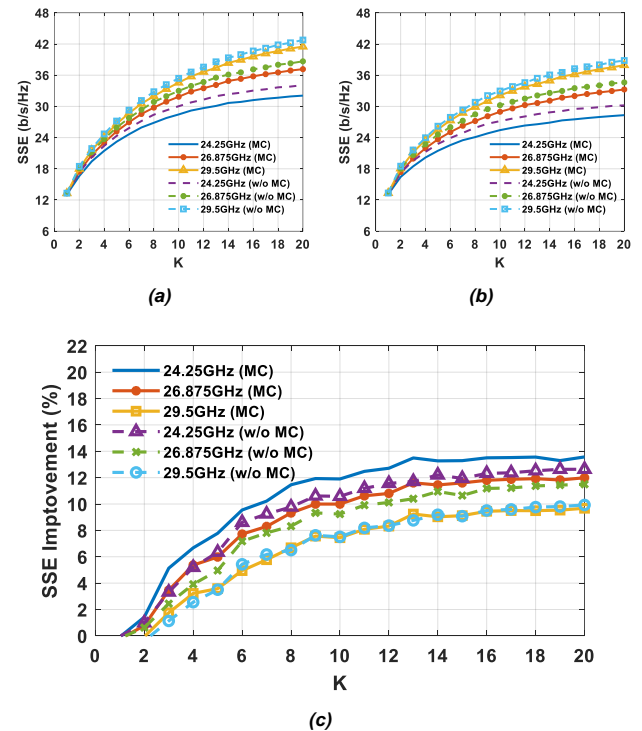

FIGURE 15. SSE comparison for a planar array composed by 8×8 elements and $\Gamma_0 = 20$ dB in case of *(a)* isosceles triangular ($\gamma = 36.6°$) lattice and *(b)* rectangular one between ideal array without MC (w/o MC) and array with MC among antenna elements. *(c)* Percentage SSE improvement comparison.

Fig. 16 shows the SINR as a function of the user (K) in case of triangular lattice. Specifically, in case of equilateral triangular lattice ($\gamma = 60°$) against square grid, the percentage SINR improvement presents a peak of around 60 % in case of four users and then it goes down with the increasing of the users. Instead, isosceles triangular lattice ($\gamma = 36.6°$) against

rectangular grid is characterized by a smoother trend as a function of the users by offering a maximum SINR improvement of 27.55 % in case of eight simultaneous served users. In case of a single user ($K = 1$) the equilateral triangular lattice provides around 16 % more of SINR improvement due to the larger average gain value inside the rectangular sector (Fig. 5). Conversely, since the isosceles triangular and rectangular lattices are characterized by comparable gain value inside the sector (Fig. 10), in case of single users they offer similar SINR.
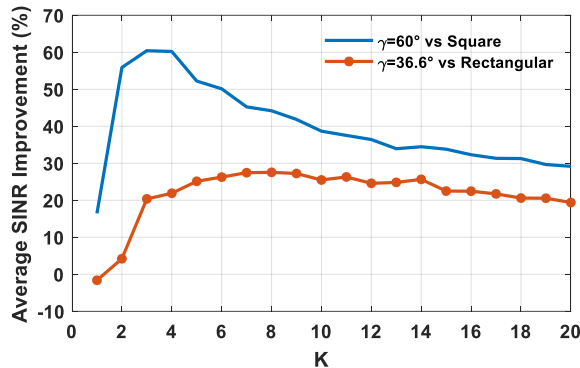

FIGURE 16. Percentage SINR improvement achieved by using triangular lattice as a function of the number of served users.

B RICIAN CHANNEL

In this scenario the contribution of few multipath rays that can exist between the users and the BS planar array has been considered through the Rician channel model [6], [50] for the evaluation of the achievable SSE. The channel matrix G between the users and the BS planar array in absence of antenna MC is modelled as:

$$G = \sqrt{\frac{r}{1+r}}G_{LOS} + \sqrt{\frac{1}{1+r}}G_{NLOS} \quad (23)$$

where the entries of G_{NLOS} matrix, that represent the NLOS components, are independent and identically distributed complex Gaussian values with zero mean and unit variance, G_{LOS} is a deterministic matrix that accounts the LOS components and the scalar $r > 0$ represents the Rician factor denoting the power ratio between LOS and NLOS.

The SSE and percentage SSE improvement as a function of the number of served users (K) for both the isosceles triangular ($\gamma = 36.6°$) and rectangular lattice in case of $r = 0$ dB and $r = 5$ dB are shown in Fig. 17 and Fig. 18, respectively. A Rician factor of 5 dB was selected since the NLOS component provides on average a power from 5 dB to 10 dB lower than LOS at mm-wave [49]. As expected, the presence of NLOS components undermines the SSE in case of MR beamforming [3]. Indeed, the achieved SSE are lower than those shown in Fig. 14 in case of LOS channel propagation. Moreover, NLOS scenario tends to reduce the advantages of adopting triangular lattice with respect to rectangular one, although it remains superior. This effect is

evident by analyzing the percentage SSE improvement with respect to rectangular lattice (Fig. 18) where the improvement tends to reduce in case of $r = 0$ dB (Fig. 18a) than $r = 5$ dB (Fig. 18b).
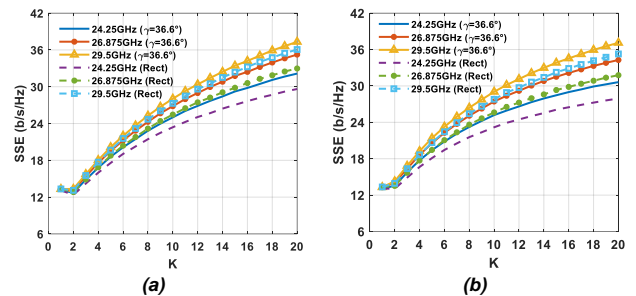

FIGURE 17. SSE comparison between isosceles triangular ($\gamma = 36.6°$) lattice and rectangular one for a planar array composed by 8×8 elements and $\Gamma_0 = 20$ dB in case of a (a) $r = 0$ dB and (b) $r = 5$ dB.

FIGURE 18. Percentage SSE improvement between isosceles triangular ($\gamma = 36.6°$) lattice and rectangular one for a planar array composed by 8×8 elements and $\Gamma_0 = 20$ dB in case of a (a) $r = 0$ dB and (b) $r = 5$ dB.

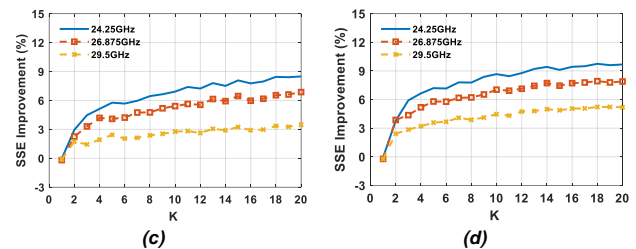To have a comprehensive view about NLOS scenario effect, the SSE as a function of r and Γ_0 is shown in Fig. 19 for both the isosceles triangular lattice ($\gamma = 36.6°$) and rectangular one in case of eight users.
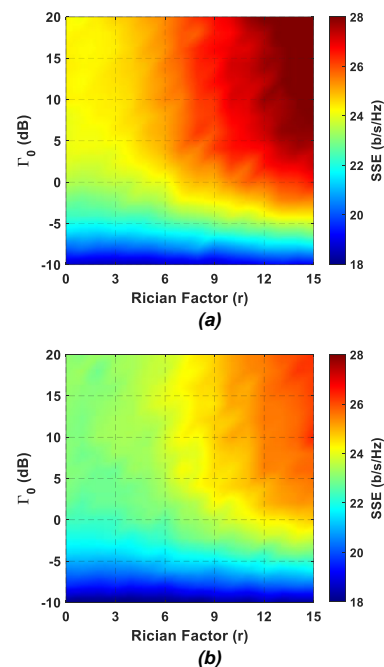

FIGURE 19. Color maps highlighting the SSE as a function of Γ_0 and the Rician factor (r) for a planar array composed by 8×8 elements at center frequency (26.875 GHz) in case of eight users; (a) isosceles triangular ($\gamma = 36.6°$) lattice and (b) rectangular one.

The color maps of Fig. 19 emphasize that the multipaths effect is more evident at high SNR where the SSE tend to gently decrease with the increasing of the NLOS power with respect to LOS. However, at noise-limited condition (low Γ_0), the Rician factor turns out to be less evident.

Fig. 20a illustrates for different frequencies the SSE in case of eight simultaneous users ($K = 8$) in an interference-limited condition (high SNR) as a function of the Rician factor (r) in dB. More in detail, it is reported in case of isosceles triangular lattice ($\gamma = 36.6°$) and rectangular where the NLOS effect is more evident. From Fig. 20b it can be inferred that at high SNR ($\Gamma_0 = 20$ dB) the percentage SSE improvement of the isosceles triangular lattice, with respect to rectangular one for eight simultaneous users, linearly decreases with the increasing of the NLOS power down to a value included from 2.6 % to 6.3 % in case of $r = 0$ dB. On the contrary, with the increasing of the Rician factor the SSE improvement linearly tend to the LOS value shown in Fig. 14 in case of eight users, namely included from 6.9 % to 11.45 %.
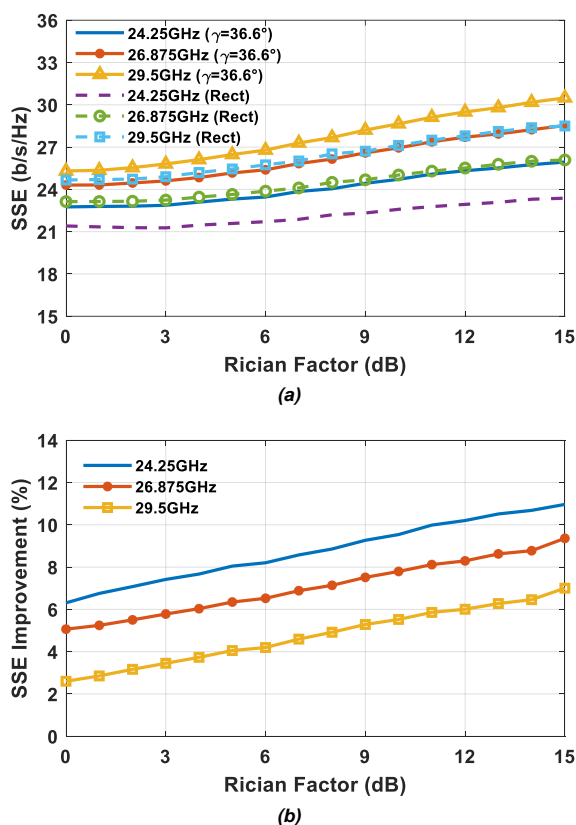

FIGURE 20. *(a)* SSE and *(b)* SSE improvement as a function of the Rician factor (*r*) in dB between isosceles triangular ($\gamma = 36.6°$) lattice and rectangular one for a planar array composed by 8×8 elements and $\Gamma_0 = 20$ dB in case of eight users.

VI. CONCLUSION

A thorough study on the employment of regular periodic lattices for planar array has been addressed in this paper with a particular focus on their applications for massive MIMO

5G systems within both the 5G NR n257 and n258 band. The results of this analysis proved beneficial effects of adopting a triangular lattice since it guarantees a drop of the ASLL, a superior angular resolution as a function of beam steering inside a defined rectangular sector as well as a lower level of MC due to a larger minimum distance (d_{min}) between elements among different planar arrays with a regular periodic lattice.

These features allow reducing both the intra-cell interference as well as the inter-cell interference. The effect of the triangular lattice shape controlled by the γ value has been also investigated in terms of gain and elements spacing.

The better robustness to interference in case of isosceles triangular lattice array layout with respect to the rectangular one has been shown even in case of multibeam antenna through the SIR in case of five users.

Afterwards, the advantage of using triangular lattice displacement of the array elements instead of square or rectangular one has been highlighted in term of SSE and SINR in case of planar array with 8×8 elements for different propagation channel scenarios.

The presented analysis proves that triangular lattice outperforms the other lattices with a uniform spacing by providing a more versatile lattice solution as a function of different predefined sector cell to serve the users. Therefore, the superior wireless performance makes triangular lattice appealing for the energy efficient massive MIMO 5G paradigm. Finally, it is reasonable to assert that these remarkable improvements can be expected even for arrays with a larger number of elements.

REFERENCES

[1] E. G. Larsson, O. Edfors, F. Tufvesson, and T. L. Marzetta, "Massive MIMO for next generation wireless systems," *IEEE Commun. Mag.*, vol. 52, no. 2, pp. 186–195, Feb. 2014, doi: 10.1109/MCOM.2014.6736761.

[2] L. Lu, G. Y. Li, A. L. Swindlehurst, A. Ashikhmin, and R. Zhang, "An Overview of Massive MIMO: Benefits and Challenges," *IEEE J. Sel. Top. Signal Process.*, vol. 8, no. 5, pp. 742–758, Oct. 2014, doi: 10.1109/JSTSP.2014.2317671.

[3] E. Björnson, J. Hoydis, and L. Sanguinetti, "Massive MIMO Networks: Spectral, Energy, and Hardware Efficiency," *Found. Trends® Signal Process.*, vol. 11, no. 3–4, pp. 154–655, 2017, doi: 10.1561/2000000093.

[4] F. A. Dicandia, S. Genovesi, and A. Monorchio, "Analysis of the Performance Enhancement of MIMO Systems Employing Circular Polarization," *IEEE Trans. Antennas Propag.*, vol. 65, no. 9, pp. 4824–4835, Sep. 2017, doi: 10.1109/TAP.2017.2723083.

[5] L. Sanguinetti, E. Bjornson, and J. Hoydis, "Toward Massive MIMO 2.0: Understanding Spatial Correlation, Interference Suppression, and Pilot Contamination," *IEEE Trans. Commun.*, vol. 68, no. 1, pp. 232–257, Jan. 2020, doi: 10.1109/TCOMM.2019.2945792.

[6] L. Sanguinetti, A. Kammoun, and M. Debbah, "Theoretical Performance Limits of Massive MIMO With Uncorrelated Rician Fading Channels," *IEEE Trans. Commun.*, vol. 67, no. 3, pp. 1939–1955, Mar. 2019, doi: 10.1109/TCOMM.2018.2884003.

[7] W. Hong *et al.*, "Multibeam Antenna Technologies for 5G Wireless Communications," *IEEE Trans. Antennas Propag.*, vol. 65, no. 12, pp. 6231–6249, Dec. 2017, doi: 10.1109/TAP.2017.2712819.

[8] J. Helander, K. Zhao, Z. Ying, and D. Sjoberg, "Performance Analysis of Millimeter-Wave Phased Array Antennas in Cellular

Handsets," *IEEE Antennas Wirel. Propag. Lett.*, vol. 15, pp. 504–507, 2016, doi: 10.1109/LAWP.2015.2455040.

[9] T. S. Rappaport *et al.*, "Millimeter Wave Mobile Communications for 5G Cellular: It Will Work!," *IEEE Access*, vol. 1, pp. 335–349, 2013, doi: 10.1109/ACCESS.2013.2260813.

[10] W. Roh *et al.*, "Millimeter-wave beamforming as an enabling technology for 5G cellular communications: theoretical feasibility and prototype results," *Commun. Mag. IEEE*, vol. 52, no. 2, pp. 106–113, 2014.

[11] Y. Kim *et al.*, "Feasibility of Mobile Cellular Communications at Millimeter Wave Frequency," *IEEE J. Sel. Top. Signal Process.*, vol. 10, no. 3, pp. 589–599, Apr. 2016, doi: 10.1109/JSTSP.2016.2520901.

[12] S. Rangan, T. S. Rappaport, and E. Erkip, "Millimeter-Wave Cellular Wireless Networks: Potentials and Challenges," *Proc. IEEE*, vol. 102, no. 3, pp. 366–385, Mar. 2014, doi: 10.1109/JPROC.2014.2299397.

[13] S. Ghosh and D. Sen, "An Inclusive Survey on Array Antenna Design for Millimeter-Wave Communications," *IEEE Access*, vol. 7, pp. 83137–83161, 2019, doi: 10.1109/ACCESS.2019.2924805.

[14] K. Kibaroglu, M. Sayginer, and G. M. Rebeiz, "A Low-Cost Scalable 32-Element 28-GHz Phased Array Transceiver for 5G Communication Links Based on a 2×2 Beamformer Flip-Chip Unit Cell," *IEEE J. Solid-State Circuits*, vol. 53, no. 5, pp. 1260–1274, May 2018, doi: 10.1109/JSSC.2018.2791481.

[15] K. Kibaroglu, M. Sayginer, T. Phelps, and G. M. Rebeiz, "A 64-Element 28-GHz Phased-Array Transceiver With 52-dBm EIRP and 8–12-Gb/s 5G Link at 300 Meters Without Any Calibration," *IEEE Trans. Microw. Theory Tech.*, vol. 66, no. 12, pp. 5796–5811, Dec. 2018, doi: 10.1109/TMTT.2018.2854174.

[16] B. Yang, Z. Yu, J. Lan, R. Zhang, J. Zhou, and W. Hong, "Digital Beamforming-Based Massive MIMO Transceiver for 5G Millimeter-Wave Communications," *IEEE Trans. Microw. Theory Tech.*, vol. 66, no. 7, pp. 3403–3418, Jul. 2018, doi: 10.1109/TMTT.2018.2829702.

[17] X. Gu *et al.*, "Development, Implementation, and Characterization of a 64-Element Dual-Polarized Phased-Array Antenna Module for 28-GHz High-Speed Data Communications," *IEEE Trans. Microw. Theory Tech.*, vol. 67, no. 7, pp. 2975–2984, Jul. 2019, doi: 10.1109/TMTT.2019.2912819.

[18] B. Sadhu *et al.*, "A 28-GHz 32-Element TRX Phased-Array IC With Concurrent Dual-Polarized Operation and Orthogonal Phase and Gain Control for 5G Communications," *IEEE J. Solid-State Circuits*, vol. 52, no. 12, pp. 3373–3391, Dec. 2017, doi: 10.1109/JSSC.2017.2766211.

[19] K. N. R. S. V. Prasad, E. Hossain, and V. K. Bhargava, "Energy Efficiency in Massive MIMO-Based 5G Networks: Opportunities and Challenges," *IEEE Wirel. Commun.*, pp. 2–10, 2017, doi: 10.1109/MWC.2016.1500374WC.

[20] Y. Aslan, J. Puskely, J. H. J. Janssen, M. Geurts, A. Roederer, and A. Yarovoy, "Thermal-Aware Synthesis of 5G Base Station Antenna Arrays: An Overview and a Sparsity-Based Approach," *IEEE Access*, vol. 6, pp. 58868–58882, 2018, doi: 10.1109/ACCESS.2018.2873977.

[21] X. Ge, R. Zi, H. Wang, J. Zhang, and M. Jo, "Multi-User Massive MIMO Communication Systems Based on Irregular Antenna Arrays," *IEEE Trans. Wirel. Commun.*, vol. 15, no. 8, pp. 5287–5301, Aug. 2016, doi: 10.1109/TWC.2016.2555911.

[22] Y. Aslan, "5G Multi-User System Simulations in Line-of-Sight With Space-Tapered Cellular Base Station Phased Arrays," p. 5, 2019.

[23] Y. Aslan, J. Puskely, A. Roederer, and A. Yarovoy, "Phase-Only Control of Peak Sidelobe Level and Pattern Nulls Using Iterative Phase Perturbations," *IEEE Antennas Wirel. Propag. Lett.*, vol. 18, no. 10, pp. 2081–2085, Oct. 2019, doi: 10.1109/LAWP.2019.2937682.

[24] Y. Aslan, J. Puskely, A. Roederer, and A. Yarovoy, "Multiple Beam Synthesis of Passively Cooled 5G Planar Arrays Using Convex Optimization," *IEEE Trans. Antennas Propag.*, vol. 68, no. 5, pp. 3557–3566, May 2020, doi: 10.1109/TAP.2019.2955885.

[25] Y. Aslan, J. Puskely, A. Roederer, and A. Yarovoy, "Trade-offs between the quality of service, computational cost and cooling

complexity in interference-dominated multi-user SDMA systems," *IET Commun.*, vol. 14, no. 1, pp. 144–151, Jan. 2020, doi: 10.1049/iet-com.2019.0206.

[26] B. Rupakula, A. H. Aljuhani, and G. M. Rebeiz, "Limited Scan-Angle Phased Arrays Using Randomly Grouped Subarrays and Reduced Number of Phase Shifters," *IEEE Trans. Antennas Propag.*, vol. 68, no. 1, pp. 70–80, Jan. 2020, doi: 10.1109/TAP.2019.2935100.

[27] N. Peccarelli, B. James, R. Irazoqui, J. Metcalf, C. Fulton, and M. Yeary, "Survey: Characterization and Mitigation of Spatial/Spectral Interferers and Transceiver Nonlinearities for 5G MIMO Systems," *IEEE Trans. Microw. Theory Tech.*, vol. 67, no. 7, pp. 2829–2846, Jul. 2019, doi: 10.1109/TMTT.2019.2914382.

[28] L. Shi, C. Bencivenni, R. Maaskant, J. Wettergren, J. Pragt, and M. Ivashina, "High-Efficiency and Wideband Aperiodic Array of Uniformly Excited Slotted Waveguide Antennas Designed Through Compressive Sensing," *IEEE Trans. Antennas Propag.*, vol. 67, no. 5, pp. 2992–2999, May 2019, doi: 10.1109/TAP.2019.2891647.

[29] S. Hussain, S.-W. Qu, W.-L. Zhou, P. Zhang, and S. Yang, "Design and Fabrication of Wideband Dual-Polarized Dipole Array for 5G Wireless Systems," *IEEE Access*, vol. 8, pp. 65155–65163, 2020, doi: 10.1109/ACCESS.2020.2984613.

[30] S. Hussain and S.-W. Qu, "A Compact Wideband, Wide-Scan Millimeter-Wave Antenna Array for 5G Wireless Applications," in *ICC 2019 - 2019 IEEE International Conference on Communications (ICC)*, Shanghai, China, May 2019, pp. 1–5, doi: 10.1109/ICC.2019.8761153.

[31] X. Ge, R. Zi, H. Wang, J. Zhang, and M. Jo, "Multi-User Massive MIMO Communication Systems Based on Irregular Antenna Arrays," *IEEE Trans. Wirel. Commun.*, vol. 15, no. 8, pp. 5287–5301, Aug. 2016, doi: 10.1109/TWC.2016.2555911.

[32] S. Zhang, X. Chen, and G. F. Pedersen, "Mutual Coupling Suppression With Decoupling Ground for Massive MIMO Antenna Arrays," *IEEE Trans. Veh. Technol.*, vol. 68, no. 8, pp. 7273–7282, Aug. 2019, doi: 10.1109/TVT.2019.2923338.

[33] B. Sadhu, X. Gu, and A. Valdes-Garcia, "Compact 28-GHz phased array antenna for 5G access," *IEEE Microw. Mag.*, vol. 20, no. 12, pp. 32–50, Dec. 2019, doi: 10.1109/MMM.2019.2941632.

[34] E. Sharp, "A triangular arrangement of planar-array elements that reduces the number needed," *IRE Trans. Antennas Propag.*, vol. 9, no. 2, pp. 126–129, Mar. 1961, doi: 10.1109/TAP.1961.1144967.

[35] R. L. Haupt, *Antenna arrays: a computational approach*. Hoboken, N.J: Wiley-IEEE Press, 2010.

[36] R. Valkonen, "Compact 28-GHz phased array antenna for 5G access," in *2018 IEEE/MTT-S International Microwave Symposium - IMS*, Philadelphia, PA, Jun. 2018, pp. 1334–1337, doi: 10.1109/MWSYM.2018.8439223.

[37] R. J. Mailloux, *Phased array antenna handbook*, 2nd ed. Boston: Artech House, 2005.

[38] H. J. Visser, *Array and Phased Array Antenna Basics: Visser/Array and Phased Array Antenna Basics*. Chichester, UK: John Wiley & Sons, Ltd, 2005.

[39] Y. Aslan, J. Puskely, A. Roederer, and A. Yarovoy, "Active Multiport Subarrays for 5G Communications," in *2019 IEEE-APS Topical Conference on Antennas and Propagation in Wireless Communications (APWC)*, Granada, Spain, Sep. 2019, pp. 298–303, doi: 10.1109/APWC.2019.8870449.

[40] E. Ali, M. Ismail, R. Nordin, and N. F. Abdulah, "Beamforming techniques for massive MIMO systems in 5G: overview, classification, and trends for future research," *Front. Inf. Technol. Electron. Eng.*, vol. 18, no. 6, pp. 753–772, Jun. 2017, doi: 10.1631/FITEE.1601817.

[41] S. Han, C. I, Z. Xu, and C. Rowell, "Large-scale antenna systems with hybrid analog and digital beamforming for millimeter wave 5G," *IEEE Commun. Mag.*, vol. 53, no. 1, pp. 186–194, Jan. 2015, doi: 10.1109/MCOM.2015.7010533.

[42] M. Hefnawi, "Hybrid Beamforming for Millimeter-Wave Heterogeneous Networks," *Electronics*, vol. 8, no. 2, p. 133, Jan. 2019, doi: 10.3390/electronics8020133.

[43] I. Ahmed *et al.*, "A Survey on Hybrid Beamforming Techniques in 5G: Architecture and System Model Perspectives," *IEEE Commun.*

Surv. Tutor., vol. 20, no. 4, pp. 3060–3097, 2018, doi: 10.1109/COMST.2018.2843719.

[44] S. Salman, Y. Aslan, J. Puskely, A. Roederer, and A. Yarovoy, "System Modeling and Simulation in 5G: A Hybrid Beamforming Approach With Power Flux Equalization in the Elevation Plane," in *2019 49th European Microwave Conference (EuMC)*, Paris, France, Oct. 2019, pp. 746–749, doi: 10.23919/EuMC.2019.8910782.

[45] M. Abdul Haleem, "On the Capacity and Transmission Techniques of Massive MIMO Systems," *Wirel. Commun. Mob. Comput.*, vol. 2018, pp. 1–9, Jul. 2018, doi: 10.1155/2018/9363515.

[46] P.- Kildal and K. Rosengren, "Correlation and capacity of MIMO systems and mutual coupling, radiation efficiency, and diversity gain of their antennas: simulations and measurements in a reverberation chamber," *IEEE Commun. Mag.*, vol. 42, no. 12, pp. 104–112, Dec. 2004, doi: 10.1109/MCOM.2004.1367562.

[47] X. Artiga, B. Devillers, and J. Perruisseau-Carrier, "Mutual coupling effects in multi-user massive MIMO base stations," in *Proceedings of the 2012 IEEE International Symposium on Antennas and Propagation*, Chicago, IL, USA, Jul. 2012, pp. 1–2, doi: 10.1109/APS.2012.6349354.

[48] Fan Yang and Y. Rahmat-Samii, "Microstrip antennas integrated with electromagnetic band-gap (EBG) structures: A low mutual coupling design for array applications," *IEEE Trans. Antennas Propag.*, vol. 51, no. 10, pp. 2936–2946, Oct. 2003, doi: 10.1109/TAP.2003.817983.

[49] I. Orikumhi, J. Kang, H. Jwa, J.-H. Na, and S. Kim, "SINR Maximization Beam Selection for mmWave Beamspace MIMO Systems," *IEEE Access*, vol. 8, pp. 185688–185697, 2020, doi: 10.1109/ACCESS.2020.3029257.

[50] S. Pratschner, T. Blazek, H. Groll, S. Caban, S. Schwarz, and M. Rupp, "Measured User Correlation in Outdoor-to-Indoor Massive MIMO Scenarios," *IEEE Access*, vol. 8, pp. 178269–178282, 2020, doi: 10.1109/ACCESS.2020.3026371.

[51] A. Yazdan, J. Park, S. Park, T. A. Khan, and R. W. Heath, "Energy-Efficient Massive MIMO: Wireless-Powered Communication, Multiuser MIMO with Hybrid Precoding, and Cloud Radio Access Network with Variable-Resolution ADCs," *IEEE Microw. Mag.*, vol. 18, no. 5, pp. 18–30, Jul. 2017, doi: 10.1109/MMM.2017.2691422.

FRANCESCO ALESSIO DICANDIA (S'16, M'20) was born in Carrara, Italy, in 1988. He received the bachelor's and master's degrees in telecommunications engineering and the Ph.D. degree in information engineering from the University of Pisa, Pisa, Italy, in 2012, 2014 and 2018, respectively. His research interests include reconfigurable antennas, characteristic modes analysis, multiple-input and multiple-output antennas, non-Foster matching network and chipless RFID sensors.

SIMONE GENOVESI (S'99-M'07-SM'19) received the Laurea degree in telecommunication engineering and the Ph.D. degree in information engineering from the University of Pisa, Pisa, Italy, in 2003 and 2007, respectively. Since 2003 he has been collaborating with the Electromagnetic Communication Laboratory, Pennsylvania State University (Penn State), University Park. From 2004 to 2006 he has been a research associate at the ISTI institute of the National Research Council of Italy (ISTI-CNR) in Pisa. During the period 2015-2017, he was several times a short-term Visiting Researcher at Grenoble Institute of Technology, Valence, France and at University Rovira I Virgili, Tarragona, Spain. He is currently an Associate Professor at "Dipartimento di Ingegneria dell'Informazione", University of Pisa. Simone Genovesi is the Coordinator of the Additive Manufacturing founded in the framework of the Departments of Excellence ("Dipartimenti di Eccellenza") funded by the Italian Ministry of Education, University and Research. Current research topics focus on radio frequency identification (RFID) systems, reconfigurable antennas and metamaterials. He is currently an Associate Editor of IEEE Transactions of Antennas and Propagation.